Meas. Sci. Technol. **19** (2008) 065405 (9pp) doi:10.1088/0957-0233/19/6/065405

Experimental investigation of the formation of acoustic streaming in a rectangular enclosure using a synchronized PIV technique

Majid Nabavi, M H Kamran Siddiqui and Javad Dargahi

Department of Mechanical and Industrial Engineering, Concordia University, 1455 de Maisonneuve Blvd West, Montreal, Quebec H3G 1M8, Canada

E-mail: m_nabav@encs.concordia.ca

Received 3 March 2008, in final form 15 April 2008
Published 19 May 2008
Online at stacks.iop.org/MST/19/065405

Abstract

The formation process of acoustic streaming generated in an air-filled rigid-walled square channel subjected to acoustic standing waves of different frequencies and intensities is investigated experimentally. The walls of the resonator are maintained at isothermal boundary condition. The synchronized particle image velocimetry (PIV) technique has been used to measure the streaming velocity fields. The results show that the formation of classical streaming patterns depends on the frequency and vibrational displacement of the acoustic driver. It is found that to generate the classical streaming flow patterns, the streaming Reynolds number $\left(Re_{s1} = u_{\max}^2 / \nu\omega\right)$ should be greater than 7.

Keywords: acoustic streaming, particle image velocimetry, acoustic standing wave, experimental investigation

1. Introduction

Nonlinear phenomena in the field of acoustics have been a matter of interest in recent years. One of these nonlinear phenomena is the acoustic streaming, a stationary fluid flow generated by sound. One type of the acoustic streaming which is always associated with a standing wave resonator is called Rayleigh streaming or outer streaming. Rayleigh streaming is a vortex-like structure outside the boundary layer generated by and superimposed on the acoustic standing wave in a closed enclosure. The interaction between the acoustic waves in a viscous fluid and the solid wall is responsible for this kind of streaming. The vortex motion generated inside the boundary layer is called Schlichting or inner streaming [1]. Rayleigh streaming can be categorized into classical (regular) and irregular streaming. The classical streaming appears as two streaming vortices per quarter wavelength of the acoustic wave which are symmetric about the channel center line. In irregular streaming, the shape and number of the streaming vortices are different from the regular case.

The phenomenon of acoustic streaming has been extensively studied using the analytical and numerical methods. Hamilton *et al* [2] derived an analytical solution for acoustic streaming generated by a standing wave in a two-dimensional channel of arbitrary width, filled with a viscous fluid. Their solution describes the inner streaming vortex confined to the boundary layer, in addition to the outer Rayleigh streaming. Moreover, it shows that the Rayleigh streaming disappears when the channel is sufficiently narrow. The two-dimensional numerical analysis of acoustic streaming induced by the finite amplitude oscillation of an air column in a closed duct has been performed by Kawahashi *et al* [3]. They concluded that the structure of acoustic streaming changes with the oscillation amplitude. When the amplitude is very small, the theoretically predicted circulatory streaming does not occur. As the amplitude increases, circulatory streaming develops and is then distorted to a complicated and irregular structure at very large oscillation amplitudes. Another notable numerical study has been performed by Aktas *et al* [4]. They simulated the acoustic streaming motion in a gas-filled

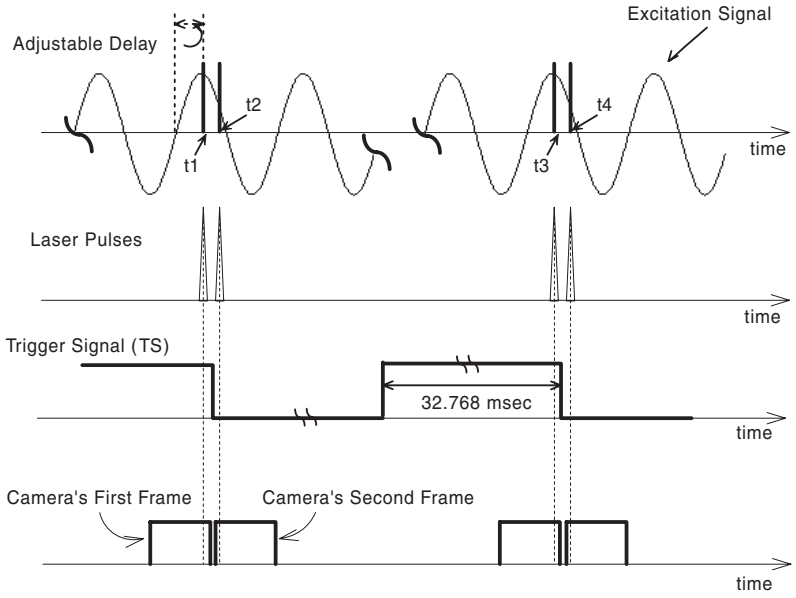

Figure 1. The triggering sequence that shows the simultaneous measurement of the acoustic and streaming velocity fields at a particular phase of the excitation signal. t_1 and t_2 correspond to the times at which the first and second images of an image pair are captured. t_3 and t_4 are the times associated with the first and second images of the consecutive image pair.

two-dimensional rectangular enclosure and investigated the effects of sound field intensity on the formation process of streaming structures. They found that up to a certain value of the enclosure height to the wavelength ratio, the vibrational motion causes classical and steady streaming flows. However, when the enclosure height is increased beyond this limit, the streaming structures become irregular and complex.

Most of the previous studies on acoustic streaming used analytical and numerical methods, and relatively few experimental investigations have been performed to measure and analyze the acoustic streaming velocity fields inside a standing wave resonator. Arroyo and Greated [5] used the stereoscopic PIV technique to measure all the three components of the streaming velocity field. However, they measured the streaming velocity field only in a region within 2 cm around the velocity node (in a 62.5 cm long tube). Hann and Greated [6] measured two components of both acoustic and streaming velocity fields simultaneously in the vicinity of a velocity node in a 70 cm long resonator excited by a 1616 Hz sinusoidal signal. It is obvious that measuring the streaming velocity only in the vicinity of a velocity node is not enough to observe the streaming structure. Thompson *et al* [7] used laser Doppler anemometry (LDA) to study the acoustic streaming generated in a cylindrical standing-wave resonator filled with air. However, the LDA measures velocity at one spatial location at a time and is not capable of simultaneously mapping the flow in a two-dimensional region. Due to the large magnitude of acoustic velocity which is superimposed on the streaming velocity, the previous PIV measurements were conducted only in the vicinity of a velocity node where the magnitude of the acoustic velocity is negligible. Recently, the authors have developed a novel approach using the synchronized PIV technique to simultaneously measure two-dimensional acoustic and streaming velocity fields at different spatial locations along a resonator and at any wave phase [8].

Although the analytical and numerical studies of the acoustic streaming are important and valuable, a comprehensive experimental study is necessary to get a better insight into the streaming velocity fields inside the standing wave resonator. In the present study, we have used the synchronized PIV technique to measure the streaming velocity fields and analyzed the formation of acoustic streaming at different acoustic frequencies and intensities. To the best of authors' knowledge, this is the first two-dimensional experimental investigation of the formation process of acoustic streaming structures inside a standing wave resonator.

2. The synchronized PIV technique

In the PIV technique, positions of the flow-tracing particles are recorded at two known times by illuminating the particles using a laser light sheet. A CCD camera captures the images of the particles at each pulse in the flow field of interest. The displacement of particles between the two images divided by the time separation between the laser pulses provides the velocity field. In the conventional PIV setup, the laser pulses are synchronized with the camera frames. Typically, these signals are not synchronized with any flow characteristics as for steady flows it is not necessary. However, for velocity measurements in the presence of acoustic standing wave, two laser pulses and the camera triggering need to be synchronized with the excitation signal to capture the velocity fields at the right phase. The authors have developed a novel approach using synchronized PIV to measure two-dimensional streaming velocity fields, in the presence of acoustic standing wave of different frequencies and intensities [8]. The basic principal of this scheme is shown in figure 1. Consider the

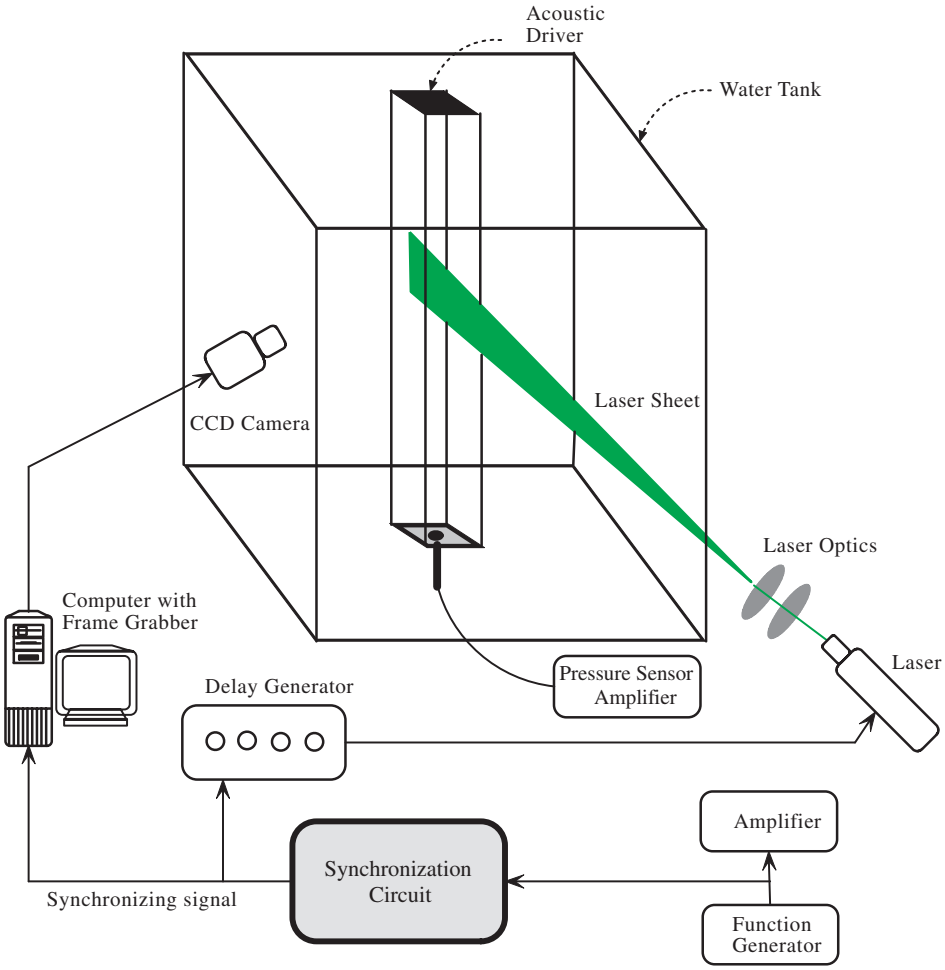

Figure 2. Schematic of the experimental setup and instrumentation.

image taken at time t_1 in figure 1 as the first image and the image taken at time t_2 as the second image, with the time separation of $t_2 - t_1$. The cross-correlation of this image pair provides the acoustic velocity field at time $(t_1 + t_2)/2$. Now, consider the image taken at time t_1 as the first image and the image taken at time t_3 as the second image, with the time separation of $t_3 - t_1$. Since the images acquired at t_1 and t_3 are exactly at the same phase, the acoustic velocity components at these times will be the same; therefore, the particle shift between these two images will only be due to streaming velocity. Thus, the cross-correlation of this image pair will provide the streaming velocity field at time $(t_1 + t_3)/2$ [8]. Trigger signal (TS) in figure 1 is used to trigger both the laser and CCD camera of the PIV system. That is, both the laser and the camera are synchronized with the excitation signal via TS. The synchronization sequence for the excitation signal, laser pulses, camera frames and trigger signal is also shown in figure 1.

3. Experimental setup

The experimental setup developed to measure the streaming velocity fields inside the standing wave tube is shown in figure 2. The acoustic chamber is a Plexiglas channel of square cross-section. The channel is 105 cm long with the inner cross-section of 4 cm × 4 cm. The walls of the channel are 10 mm thick, therefore, the assumption of rigid walls held for this channel. The two-dimensional velocity fields inside the channel are measured using synchronized PIV. A New Wave Research 120 mJ Nd:YAG laser is used as a light source for the PIV measurements. A digital 2 megapixel progressive scan CCD camera (JAI CV-M2) with the resolution of 1600 × 1200 pixels is used to image the flow. The camera is connected to a PC equipped with a frame grabber (DVR Express, IO Industries, London, ON, Canada) that acquired 8 bit images at a rate of 30 Hz. A four-channel digital delay generator (555-4C, Berkeley Nucleonics Corporation, San Rafael, CA) is used to control the timing of the laser pulses. Bis(2-ethylhexyl) sebacate mist with the mean diameter of 0.5 μm is used as the tracer particles. An aerosol generator (Lavision Inc., Ypsilanti, MI) is used to generate the mist. The acoustic pressure is measured by a condenser microphone cartridge Model 377A10 PCB Piezotronics. The microphone consists of a microphone cartridge and a microphone preamplifier. A preamplifier Model 426B03 is used in order to measure the sound pressure level. The frequency response is almost flat

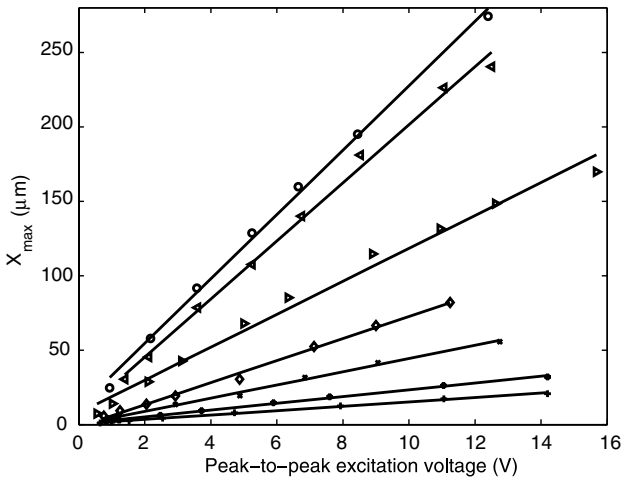

Figure 3. Maximum vibrational displacement (X_{max}) at the center of the driver diaphragm versus excitation voltage for different excitation frequencies: ○, 340 Hz; ◁, 400 Hz; ▷, 508 Hz; ◇, 680 Hz; ×, 1020 Hz; ∗, 1360 Hz; +, 1704 Hz. Solid line, linear fit.

between 5 Hz and 100 kHz. During velocity measurements, the microphone is placed inside a hole at the end wall of the channel (see figure 2). Thus, the microphone measured the maximum pressure fluctuation. A special loudspeaker driver is used to excite the acoustic standing wave inside the tube. The driver has the maximum power of 200 W. A function generator (model Agilent 33120A) is used to generate the sinusoidal wave. The accuracy of the generated frequency and amplitude are 1 μHz and 0.1 mV, respectively. The signal from the function generator is amplified by a 220 W amplifier (Pioneer SA-1270). The loudspeaker is driven by this amplified signal (see figure 2).

The resonator is filled with air ($c_0 = 344$ m s^{-1}). As shown in figure 2, we have put the resonator inside a large water tank of 50 × 50 × 90 cm dimensions, in order to completely isolate the resonator from the temperature gradients within the laboratory that can cause ambient convection velocities and affect the streaming patterns. The water temperature is $T = 22.5 \pm 0.1\,^{\circ}$C. Since water has a large heat capacity, its temperature remains constant. Therefore, the isothermal boundary condition all around the resonator is satisfied.

The maximum vibrational displacement of the acoustic driver is also measured for each excitation amplitude and frequency. A Brüel & Kjær laser vibrometer is used to measure this parameter. Figure 3 shows the maximum vibrational displacement at the center of the driver's diaphragm as a function of the excitation voltage for different excitation frequencies. The plot shows that for a given excitation frequency, the vibrational displacement and excitation voltage are linearly related. Using figure 3 for a given excitation frequency, we can estimate the vibrational displacement of the driver at all excitation voltages over the range of our practical interest.

Shin *et al* [9] estimated the uncertainty in the PIV measurements of the acoustic velocity fields based on the response time of the tracer particles. We used the same approach in the present study. The characteristic response time

Table 1. The cases considered for the acoustic streaming experiments along with the details of parameters for each case. f, frequency; ℓ, half-wavelength; H/ℓ, normalized channel width; X_{max}, maximum vibrational displacement of the driver.

Case	f (Hz)	$\ell = \lambda/2$ (cm)	H/ℓ	X_{max} (μm)	X_{max}/ℓ
A-1	666	25.8	0.15	12	4.65×10^{-5}
A-2	666	25.8	0.15	23	8.91×10^{-5}
A-3	666	25.8	0.15	35	1.36×10^{-4}
A-4	666	25.8	0.15	120	4.65×10^{-4}
B-1	976	17.6	0.23	20	1.13×10^{-4}
B-2	976	17.6	0.23	28	1.58×10^{-4}
B-3	976	17.6	0.23	43	2.44×10^{-4}
B-4	976	17.6	0.23	96	5.45×10^{-4}
C-1	1310	13.1	0.3	12	9.14×10^{-5}
C-2	1310	13.1	0.3	20	1.52×10^{-4}
C-3	1310	13.1	0.3	42	3.20×10^{-4}
C-4	1310	13.1	0.3	80	6.09×10^{-4}

of the seed particles is computed by $T_p = u_T/g$, where T_p is the particle response time, u_T is the particle terminal velocity and g is the acceleration due to gravity [10]. The terminal velocity is computed by $u_T = (\gamma - 1)D^2 g/18\nu$, where D is the diameter of the tracer particles, ν is the kinematic viscosity of the fluid and γ is the ratio of the density of particle to the density of fluid [11]. Using the above equations, for $D = 0.5$ μm and $u_T = 6.5$ μm s^{-1}, the particle response time is found to be $T_p = 0.67$ μs. For the driver frequency of 1000 Hz, the particle response is more than 1500 times faster than the wave period. Thus, we conclude that the tracer particles accurately follow the flow.

For PIV cross-correlation, the size of the interrogation region is set equal to 32 × 32 pixels and the size of the search region is set equal to 64 × 64 pixels. A 50% window overlap is used in order to increase the nominal resolution of the velocity field to 16 × 16 pixels. A three-point Gaussian sub-pixel fit scheme is used to obtain the correlation peak with sub-pixel accuracy.

For each set of measurements, 200 PIV images are captured. From these images, 100 acoustic velocity fields and 50 streaming velocity fields are computed using the technique described in section 2. The spurious velocity vectors are detected and then corrected using a local median test [12].

4. Results and discussions

In this study, we have considered three different excitation frequencies (f) and four different maximum vibrational displacements (X_{max}) of the acoustic driver for each frequency. That is, a total of 12 different cases are considered which are summarized in table 1. The half-wavelength of the acoustic standing wave (ℓ), normalized channel width (H/ℓ) and normalized maximum vibrational displacement (X_{max}/ℓ) are also listed in table 1.

In cases A-1 to A-4, the frequency of the acoustic driver is set equal to 666 Hz. The half-wavelength (ℓ) of the acoustic standing wave corresponding to this frequency is 25.8 cm. It allows the formation of two full standing waves inside the

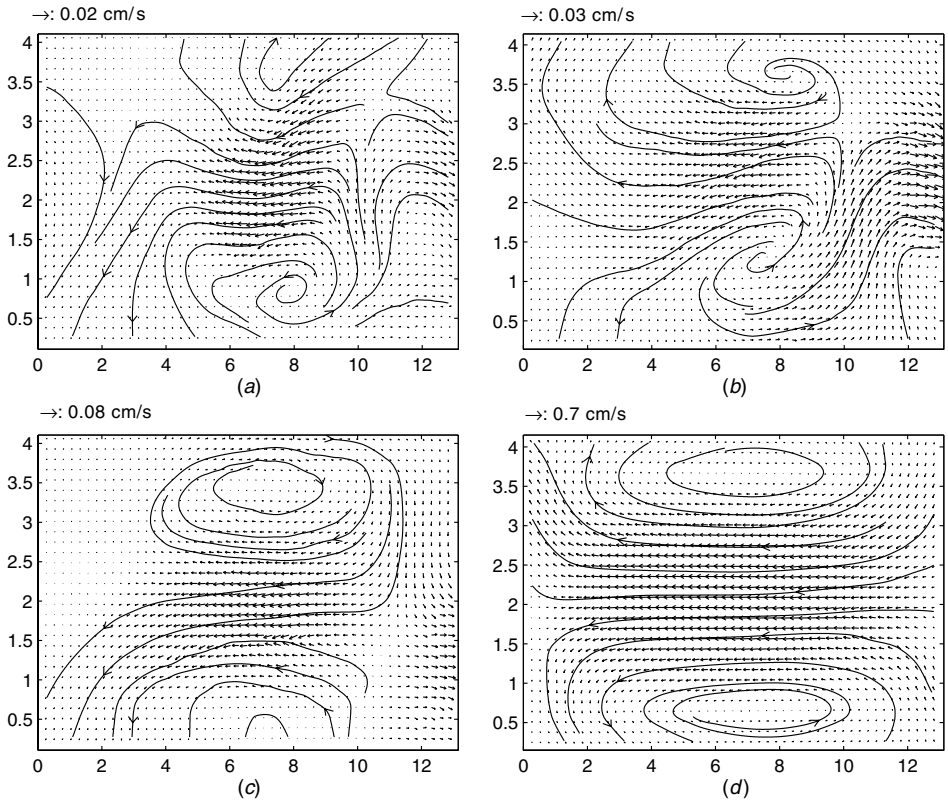

Figure 4. The streaming structures in the half-wavelength region for (*a*) case A-1, (*b*) case A-2, (*c*) case A-3, (*d*) case A-4. The horizontal axis is *x* in cm and the vertical axis is *y* in cm.

channel. The field of view of the CCD camera is set in a way to map the flow field in the half-wavelength section. That is, the field of view of the camera is set equal to 13.1 cm in horizontal and 9.8 cm in vertical. The maximum vibrational displacement ($X_{\max}$) is 12, 23, 35 and 120 μm, for cases A-1 to A-4, respectively. The maximum peak-to-peak pressure amplitudes at pressure anti-node (P_{ac}) are 375, 575, 720 and 2187 Pa for cases A-1 to A-4, respectively.

The streaming flow patterns for cases A-1 to A-4 are shown in figures 4(*a*)–(*d*), respectively. The streamlines are also depicted in the figures for better flow visualization. The sequence shows the impact of excitation amplitude on the structure of the streaming flow as it increases from case A-1 to case A-4. The classical streaming structure is typically comprised of two streaming vortices per quarter wavelength of the acoustic wave which are symmetric about the channel center line. The plot in figure 4(*a*) shows that at smaller excitation amplitude (case A-1), some flow circulations are visible but they are not similar to the classical streaming structure. As the excitation magnitude further increased (figure 4(*b*), case A-2), two vortices appear to be establishing themselves in the quarter wavelength. However, they are not symmetric and fully developed. At a higher excitation magnitude (figure 4(*c*), case A-3), two classical and symmetric streaming patterns are almost established. At a further higher excitation magnitude (case A-4), the classical outer streaming vortices are clearly observed (see figure 4(*d*)). Kawahashi *et al* [3] argued that the maximum vibrational displacement

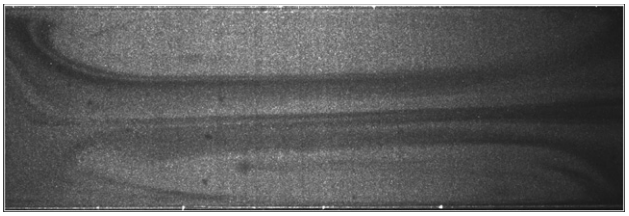

Figure 5. A sample of PIV image for case A-4.

of the acoustic driver plays an important role in the formation of classical streaming vortices. The present results confirm their argument by showing that for cases A-1 and A-2, the maximum vibrational displacement of the driver is not large enough to generate a perfect classical streaming structure. For a better qualitative observation of the streaming patterns, a sample PIV image for case A-4 is shown in figure 5. The image shows two nearly symmetric and developed Rayleigh or outer streaming vortices.

For the next experimental set, the frequency of the acoustic driver is increased to 976 Hz. This results in the formation of three full standing waves inside the channel. The field of view of the camera is set equal to 10.6 cm in horizontal and 8 cm in vertical to map the flow field in the quarter wavelength section of the channel. Four cases are considered in this set (cases B-1 to B-4) which correspond to the maximum vibrational displacement of the acoustic driver ($X_{\max}$) equal to 20 μm, 28 μm, 43 μm and 96 μm, respectively.

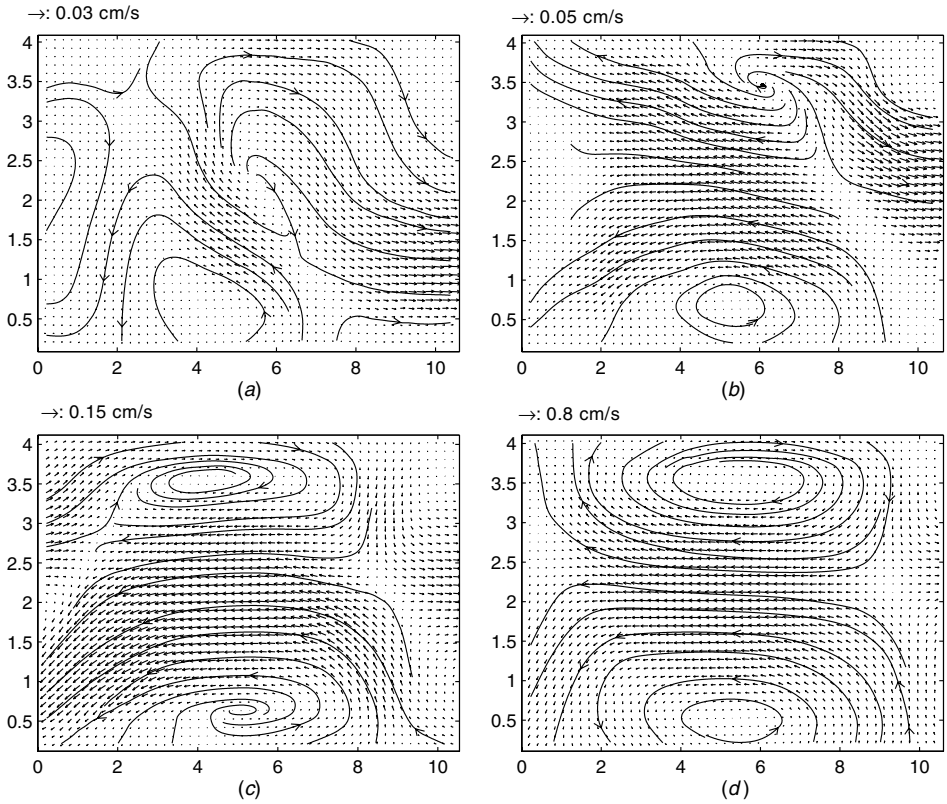

Figure 6. The streaming structures in the quarter-wavelength region for (*a*) case B-1, (*b*) case B-2, (*c*) case B-3, (*d*) case B-4. The horizontal axis is x in cm and the vertical axis is y in cm.

The maximum peak-to-peak pressure amplitudes at pressure anti-node (P_{ac}) are 500, 690, 962 and 2300 Pa for cases B-1 to B-4, respectively.

Figure 6 depicts the streaming velocity fields for these four cases. The plots show that the classical streaming structure, i.e. two symmetric vortices in quarter wavelength is clearly observed for cases B-3 and B-4. For cases B-1 and B-2, the plot shows that the classical streaming vortices are not completely developed which would be due to the reason that the acoustic intensity is not strong enough in these cases.

The final set of experiments is conducted at the driver frequency of 1310 Hz resulting in the formation of four complete standing waves inside the channel. Four cases are considered in this set (cases C-1 to C-4) which correspond to $X_{\max} = 12$, 20, 42 and 80 μm, respectively. The camera field of view is set equal to 13.1 cm in horizontal and 9.8 cm in vertical that allows us to capture the streaming velocity field in the half-wavelength region. The maximum peak-to-peak pressure amplitudes at pressure anti-node (P_{ac}) are 513, 812, 1375 and 2188 Pa for cases C-1 to C-4, respectively.

The streaming flow structures for cases C-1 to C-4 are shown in figure 7. The plots show that for cases C-1 and C-2, the streaming flow patterns are not developed, whereas, for cases C-3 and C-4, the classical streaming patterns, i.e. four vortices per half-wavelength of the standing wave which are symmetric about the channel center line, are observed. The reason for underdeveloped streaming patterns for cases C-1 and C-2 would be the same as for previous cases, namely that $X_{\max}$ is not large enough.

The accuracy of the synchronized PIV technique to measure the streaming velocities inside the acoustic resonator has already been verified by the authors [8]. To further confirm that the experimental streaming velocities are accurate enough, they are compared with the analytical velocities from the exact solution of the linear wave equation. The amplitude of the axial component of the acoustic velocity field in the linear case is given as $u = u_{\max} \sin(2\pi x/\lambda)$, where x is the axial coordinate. The axial component of the streaming velocity field (u_{st}) is

$$u_{st} = \frac{3}{8}\frac{u_{\max}^2}{c}\left(1 - \frac{2y^2}{(H/2)^2}\right)\sin(\pi x/\ell), \qquad (1)$$

where y is the transverse coordinate ($-H/2 \leqslant y \leqslant H/2$), H is the width of the tube and $\ell = \lambda/4$ [7]. The theoretical and experimental root-mean-squares (RMS) of the axial component of the streaming velocity (u_{strms}) along the resonator for cases A-4, B-4 and C-4 (in which the classical streaming patterns are established) are quantitatively compared in figure 8. The plots show that the variation of the axial component of the streaming velocity with respect to the axial coordinate is sinusoidal. The relative errors between the experimental and analytical mean values of u_{strms} for cases A-4, B-4 and C-4 are 11%, 6.5% and 10.5%, respectively. Good agreement between the analytical and experimental results confirms that the presented streaming patterns are accurate.

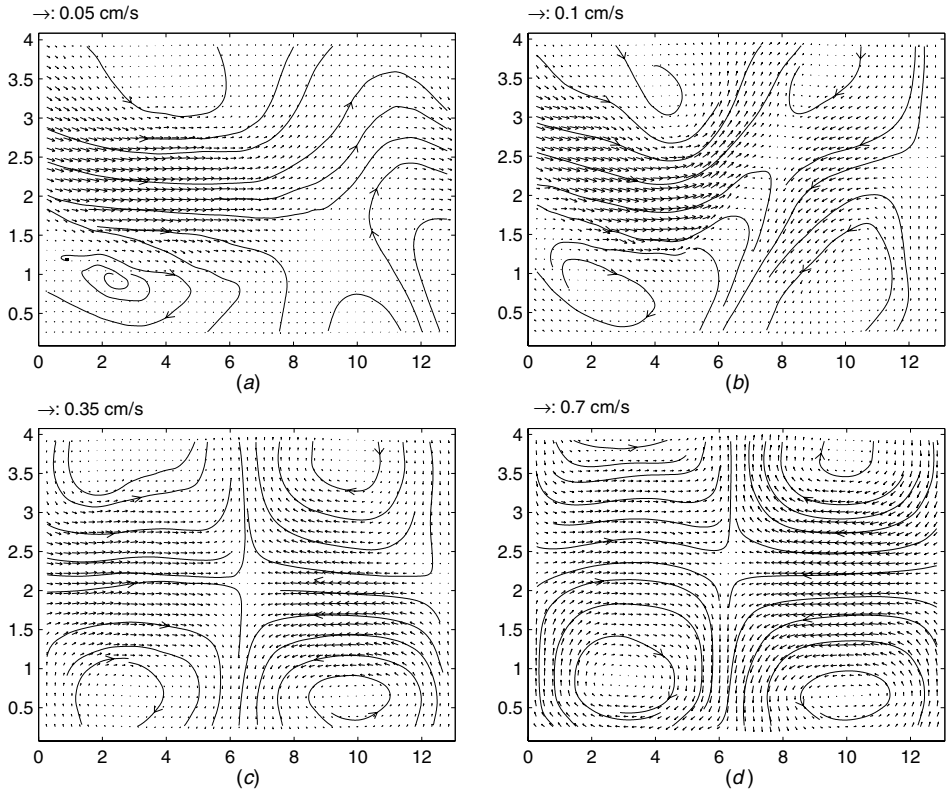

Figure 7. The streaming structures in the quarter-wavelength region for (*a*) case C-1, (*b*) case C-2, (*c*) case C-3, (*d*) case C-4. The horizontal axis is x in cm and the vertical axis is y in cm.

The phased-averaged two-dimensional acoustic velocity field, averaged over 100 fields, for case C-4 over the half of the wavelength at $t/T = 0.167$ is shown in figure 9. The calculated mean standard deviation of the axial acoustic velocity across the 100 velocity fields is 4.75 cm s^{-1}, which is 3.4% of the mean axial acoustic velocity (139 cm s^{-1}). The plot, as expected, shows the maximum acoustic velocity at the velocity anti-node located at $x = \lambda/4$. The theoretical and experimental mean acoustic velocities along the resonator for case C-4 at time $t/T = 0.167$ are depicted in figure 10, which are in good agreement in both amplitude and shape.

We have presented the results for three excitation frequencies and different displacement amplitudes of the acoustic driver. It should be noted that for all cases considered in this study, the streaming patterns are found to be stationary and time invariant. In the following, we have attempted to generalize the results obtained in the present study. Two frequently used definitions of the streaming Reynolds number are

$$Re_{s1} = u_{\max}^2 \big/ \nu\omega, \tag{2}$$

and

$$Re_{s2} = \frac{1}{2}\left(\frac{u_{\max}}{c}\right)^2 \left(\frac{H}{\delta_\nu}\right)^2, \tag{3}$$

where ν is the kinematic shear viscosity, $\omega = 2\pi f$ and $\delta_\nu = \sqrt{2\nu/\omega}$ is the thickness of the viscous boundary layer. Aktas *et al* [4] have used Re_{s1} in their numerical study of acoustic streaming and Thompson *et al* [7] have used Re_{s2} in their acoustic streaming measurement. Re_{s1} and Re_{s2} for all cases considered in the present study are presented in table 2. The results show that for cases A-1 to A-4 ($f = 666$ Hz), the classical streaming is observed at $Re_{s1} > 6.43$. At $f = 976$ Hz (cases B-1 to B-4) the classical streaming is observed at $Re_{s1} > 6.28$, whereas at $f = 1310$ Hz (cases C-1 to C-4), it is observed at $Re_{s1} > 6.53$. The results also show that for all cases considered, the classical

Table 2. Different experimentally obtained parameters for the cases studied. P_{ac}, maximum peak-to-peak pressure; $u_{\max}$, maximum acoustic velocity; Re_{s1} and Re_{s2}, two definitions of acoustic Reynolds number.

Case	P_{ac} (Pa)	$u_{\max}$ (m s^{-1})	Re_{s1}	Re_{s2}	Streaming pattern
A-1	375	0.42	2.73	0.16	Non-developed
A-2	575	0.65	6.43	0.38	Non-developed
A-3	720	0.81	10.04	0.91	Classical
A-4	2187	2.46	93.0	5.51	Classical
B-1	500	0.56	3.29	0.42	Non-developed
B-2	690	0.78	6.28	0.80	Non-developed
B-3	962	1.08	12.3	1.56	Classical
B-4	2300	2.59	70.2	8.92	Classical
C-1	513	0.60	2.79	0.64	Non-developed
C-2	812	0.92	6.53	1.49	Non-developed
C-3	1375	1.55	18.7	4.28	Classical
C-4	2188	2.47	47.3	10.83	Classical

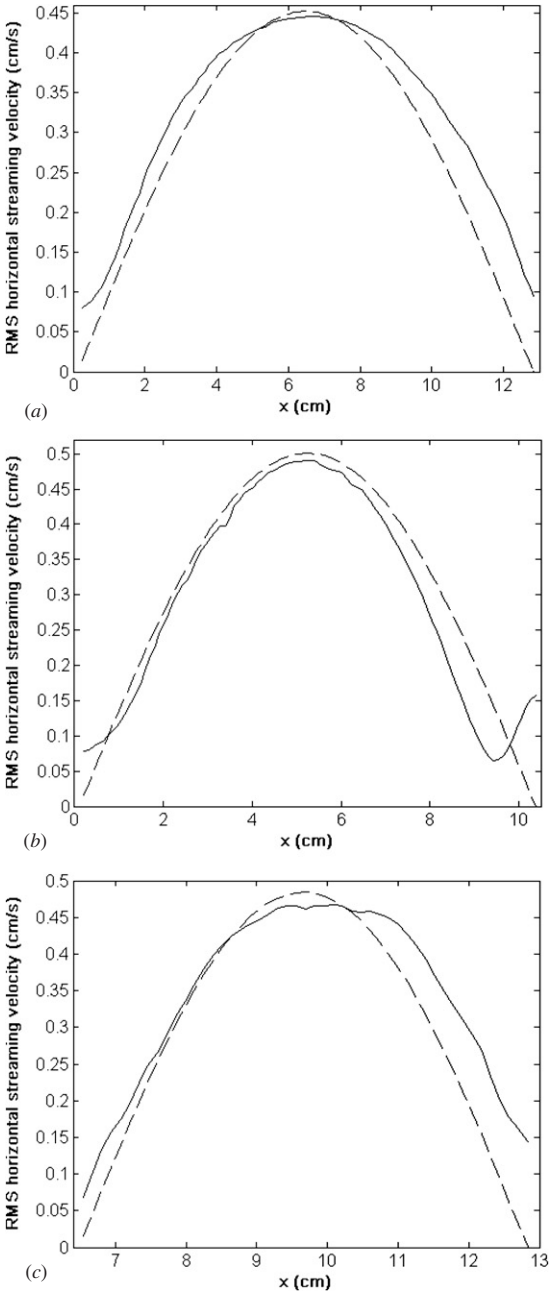

Figure 8. The theoretical (dashed line) and experimental (solid line) RMS of the axial component of the streaming velocity (u_{strms}) along the resonator for cases (*a*) A-4, (*b*) B-4 and (*c*) C-4 in which the classical streaming patterns are established.

streaming is not developed for $Re_{s1} < 7$. However, as observed in table 2, Re_{s2} does not appear to be an appropriate parameter to classify non-developed and classical streaming patterns. While classical streaming is observed in case A-3 at $Re_{s2} = 0.91$, the streaming patterns are still in developing stage at $Re_{s2} = 1.49$ for case C-2. Thus, based on the present data, it can be concluded that the streaming patterns can be classified based on Re_{s1} and that the classical streaming patterns are established at $Re_{s1} > 7$.

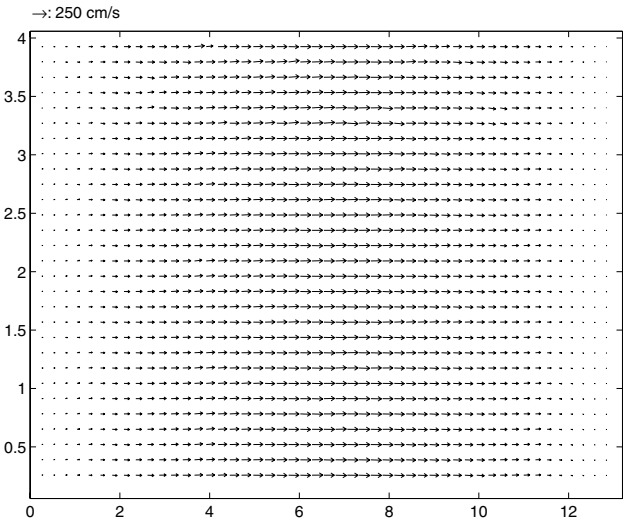

Figure 9. Experimental phased-averaged acoustic velocity field for case C-4 at $t/T = 0.167$. $x = 0$ and $x = 13.1$ cm correspond to the velocity nodes and $x = 6.55$ cm corresponds to the velocity anti-node. Note that the resolution of the velocity vectors was reduced to half in the plot for better visualization.

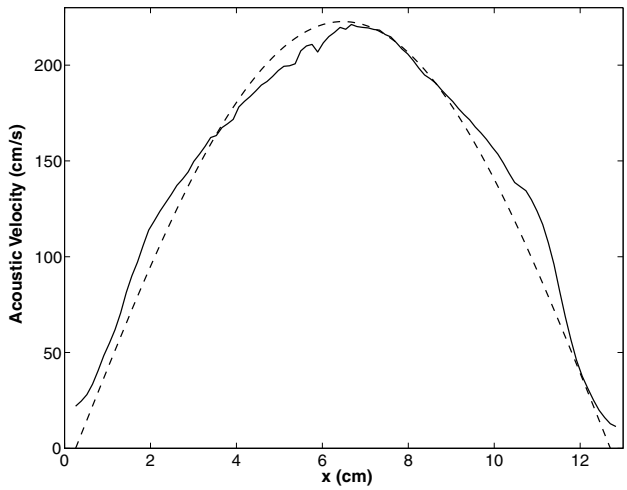

Figure 10. The theoretical (dashed line) and experimental (solid line) values of mean acoustic velocity along the resonator for case C-4 at time $t/T = 0.167$.

Thompson *et al* [7] have measured classical streaming in a channel with $H = 4.8$ cm, $u_{\max} = 0.81$ m s^{-1} and $f = 311$ Hz. Based on equation (2), the streaming Reynolds number for their case is $Re_{s1} = 21.5$. This is in agreement with the condition $Re_{s1} > 7$. Furthermore, based on equation (3), we have observed classical streaming at $Re_{s2} > 1.49$ for $f = 1310$ Hz, at $Re_{s2} > 0.8$ for $f = 976$ Hz, and at $Re_{s2} > 0.38$ for $f = 666$ Hz. As seen, by decreasing the excitation frequency, classical streaming is established at lower values of Re_{s2}. Therefore, at $f = 311$ Hz used in [7], the classical streaming is established at Re_{s2} much less than 0.38. Thompson *et al* [7] have measured classical streaming at $Re_{s2} = 0.36$ for $f = 311$ Hz, which is in agreement with our results. The lowest value of Re_{s1} in which Aktas *et al* [4] predicted classical streaming using their numerical

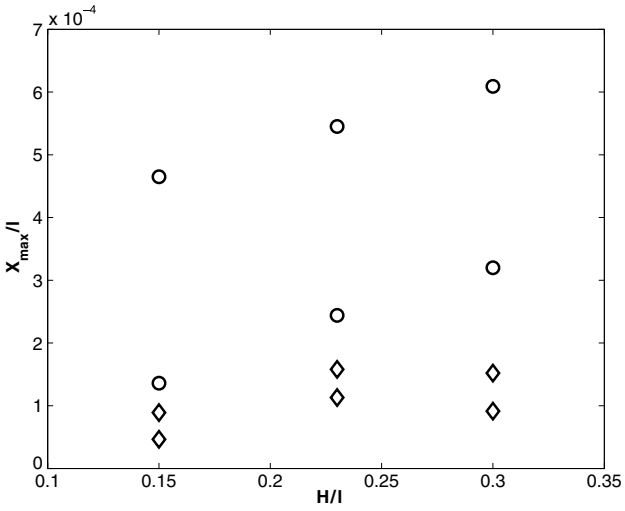

Figure 11. The normalized channel width (H/ℓ) versus the normalized maximum vibrational displacement ($X_{\max}/\ell$) for all cases; ⋄, non-developed streaming structures; ○, classical streaming structures.

scheme is 6.6, which is very close to our threshold streaming Reynolds number ($Re_{s1} > 7$). Therefore, our experimental results are in agreement with the numerical predictions of Aktas *et al* [4] and experimental measurements of Thompson *et al* [7].

Finally, using the results summarized in table 2, the non-developed and classical streaming flow patterns can also be classified based on the normalized channel width (H/ℓ) and the normalized maximum vibrational displacement ($X_{\max}/\ell$). The normalized channel width (related to the vibrational frequency) versus the normalized maximum vibrational displacement (related to both vibrational displacement and frequency) is plotted in figure 11. The symbol (⋄) indicates the streaming structures which are not developed. The classical streaming patterns are symbolized by (○). Figure 11 clearly shows that both the vibrational amplitude and frequency affect the classical streaming structure. Using numerical simulations, Kawahashi *et al* [3] and Aktas *et al* [4] also found that the streaming structure can be affected by the vibrational amplitude and frequency. As shown in figure 11, for $H/\ell = 0.15$ ($f = 666$ Hz, cases A-1 to A-4), if the normalized maximum vibrational displacement ($X_{\max}/\ell$) is greater than about 0.0001, we observe classical streaming structures, and for the values of $X_{\max}/\ell$ less than this number, streaming flow patterns are in developing state and they are not completely developed. This threshold number for $H/\ell = 0.23$ ($f = 976$ Hz, cases B-1 to B-4) and $H/\ell = 0.3$ ($f = 1310$ Hz, cases C-1 to C-4) is about 0.000 16.

5. Conclusions

Experimental investigation of the formation of acoustic streaming velocity fields in an air-filled rigid-walled square channel subject to acoustic standing waves is performed using the synchronized PIV technique. The resonator has been put inside a large water tank in order to completely isolate the resonator from the temperature gradients within the laboratory that can cause ambient convection velocities. The effects of the frequency and maximum vibrational displacement of the acoustic driver on the streaming structure are studied. The results show that for a given vibrational frequency, classical streaming structures are observed only when the vibrational displacement of the acoustic driver is sufficiently large. The results also show that for the generation of classical streaming flow patterns, the streaming Reynolds number (Re_{s1}) should be greater than 7. It is also observed that the formation of classical streaming patterns also depends on the frequency and vibrational displacement of the acoustic driver. The experimentally obtained structures of streaming velocity fields are found to be in good agreement with the theoretical ones and previously reported numerical predictions and experimental measurements.

Acknowledgments

This research is funded by the grants from Natural Science and Engineering Research Council of Canada (NSERC) and Concordia University.

References

[1] Boluriaan S and Morris P J 2003 Acoustic streaming: from Rayleigh to today *Int. J. Aeroacoust.* **2** 255–92
[2] Hamilton M F, Ilinskii Y A and Zabolotskaya E A 2003 Acoustic streaming generated by standing waves in two-dimensional channel of arbitrary width *J. Acoust. Soc. Am.* **113** 153–60
[3] Kawahashi M and Arakawa M 1996 Nonlinear phenomena induced by finite amplitude oscillation of air-column in closed duct *JSME Int. J.* **39** 280–6
[4] Aktas M K and Farouk B 2004 Numerical simulation of acoustic streaming generated by finite-amplitude resonant oscillations in an enclosure. *J. Acoust. Soc. Am.* **116** 2822–31
[5] Arroyo M P and Greated C A 1991 Stereoscopic particle image velocimetry *Meas. Sci. Technol.* **2** 1181–6
[6] Hann D B and Greated C A 1997 The measurement of flow velocity and acoustic particle velocity using particle image velocimetry *Meas. Sci. Technol.* **8** 1517–22
[7] Thompson M W and Atchley A A 2005 Simultaneous measurement of acoustic and streaming velocities in a standing wave using lase Doppler anemometry *J. Acoust. Soc. Am.* **117** 1828–38
[8] Nabavi M, Siddiqui M H K and Dargahi J 2007 Simultaneous measurement of acoustic and streaming velocities using synchronized PIV technique *Meas. Sci. Technol.* **18** 1811–17
[9] Shin Y, Jaewon C and Domoto G A 2005 Compressible flow of liquid in a standing wave tube *J. Fluid Mech.* **536** 321–45
[10] Snyder W H and Lumley J L 1971 Some measurements of particle velocity autocorrelation functions in a turbulent flow *J. Fluid Mech.* **48** 41–71
[11] Siegel D A and Plueddemann A J 1991 The motion of a solid sphere in an oscillating flow: an evaluation of remotely sensed Doppler velocity estimates in the sea *J. Atmos. Oceanic Technol.* **8** 296–304
[12] Siddiqui M H K, Loewen M R, Richardson C, Asher W E and Jessup A T 2001 Simultaneous particle image velocimetry and infrared imagery of microscale breaking waves *Phys. Fluids* **13** 1891–903